
# Wire plus arc additive manufactured functional steel surfaces enhanced by rolling

Philip Dirisu, Ganguly Supriyo, Filomeno Martina, Xiangfang Xu, Stewart Williams

PII: S0142-1123(19)30341-X
DOI: https://doi.org/10.1016/j.ijfatigue.2019.105237
Reference: JIJF 105237

To appear in: *International Journal of Fatigue*

Received Date: 17 December 2018
Revised Date: 17 August 2019
Accepted Date: 19 August 2019

Please cite this article as: Dirisu, P., Supriyo, G., Martina, F., Xu, X., Williams, S., Wire plus arc additive manufactured functional steel surfaces enhanced by rolling, *International Journal of Fatigue* (2019), doi: https://doi.org/10.1016/j.ijfatigue.2019.105237

International Journal of Fatigue, Volume 130, January 2020, Article number 105237
DOI:10.1016/j.ijfatigue.2019.105237



# Wire plus arc additive manufactured functional steel surfaces enhanced by rolling

**Philip Dirisu,* Ganguly Supriyo, Filomeno Martina, Xiangfang Xu, Stewart Williams**

Welding Engineering and Laser Processing Centre, Cranfield University, Cranfield MK43 0AL, UK.

* Correspondence: taiye.p.dirisu@cranfield.ac.uk; Tel.: +44-777-6644-897

## Abstract:

Surface waviness (SW) is one of the major problems confronting the economical use of as-deposited components made with the wire plus arc additive manufactured (WAAM) process. The SW acts as a stress raiser, thereby reducing the tensile properties and fatigue life of the component. In this study, the effect of compressive residual stress on the mechanical and fatigue behaviour of the as-deposited WAAM mild steel component was carried out using a hybrid process which combines deposition and rolling on the WAAM component surface. The fractured faces and microstructure were characterised by a scanning electron and optical microscope. The microstructural changes were characterised by X-ray diffraction techniques. The results revealed that an increase in the notch radius and compressive stress induced by rolling on the as-deposited condition reduced the SW from 0.18 to 0.08 mm with an increase in the dislocation clusters and consequently retarding the crack propagation rate and improving fatigue life. This work shows that rolling has a dual effect on as-deposited WAAM mild steel components with a new functional surface.

**Keywords**: functional surfaces; fatigue life; tensile strength; WAAM; rolling.

## 1. Introduction

Currently, offshore and onshore wind energy generation constitute about 8.01% and 9.1% of the entire energy generation in the UK, respectively. This has led to the reduction of $CO_2$ emissions in the UK by 12 million tonnes [1]. The Vision 2020 projection of the UK Department of Energy and Climate Change is to reduce further $CO_2$ emissions by 10% by the year 2020 [2]. With this mandate, the wind turbine original equipment manufacturers (OEMs) must look for solutions and cutting-edge technologies to remain at a competitive advantage over other forms of energy producers. The current subtractive manufacturing (SM) process used in the mainframe and hub

has some drawbacks such as material wastage, increased cost and higher production lead time of materials manufactured through a sand casting process before machining.

Additive manufacturing (AM) is a method of building parts and components, layer by layer using different energy sources. The development of AM processes has been on the increase because of their numerous advantages compared to SM. The use of AM can drastically reduce material wastage and production lead times while allowing the building of complex shapes with less expensive tooling requirements and hence cost savings [3–6]. AM methods have been developed in recent times to optimise geometrical features, deposition rates, dimensional accuracy, layer thickness and surface finish [7]. Despite all these improvements, only a rough near net shaped surface (final outlook finish) can be produced [8].

One of the newest low-cost AM processes is wire plus arc additive manufacture (WAAM), which involves building a structure with a consumable wire in a layer by layer manner in an open or atmospherically controlled chamber. The WAAM process has a higher deposition rate than other AM processes, close to 10Kg/hr for steels [9,10], with better material utilisation rate than others but has a limited ability to produce finer surface finish features [11]. Rougher surface finish in WAAM is a result of overheating and heat accumulation effects which reduce the surface tension and make the molten pool unstable. The WAAM process parameters such as travel speed (TS), wire feed speed (WFS), interpass temperatures and the ratio of WFS to TS are responsible for the heat accumulation effects [12–14]. Besides, the SW challenges, WAAM has been known to be affected by unevenly distributed stresses generated during deposition, which might require further post-heat treatment or cold work to relieve these stresses and improve their mechanical properties [15]. Path planning and deposition strategies compensation with built parameter optimisation have been effective in reducing the residual stresses [16,17]**.** A 500µm surface waviness (SW) encountered in WAAM is a serious problem, limiting the use of WAAM as-deposited structures [5]. The as-deposited state with an SW of 500µm leads to a high level of geometric stress concentration, which will limit the use of the component in the as-deposited state for applications where a component is subjected to dynamic loading. Despite these drawbacks, the low-cost WAAM AM process remains the most suited for large scale part manufacturing because of its higher deposition rate capabilities, unique mechanical properties better than powder bed systems, better material utilisation and low equipment cost [5,18].

It is important to know that wetting plus spreading and re-melting are the two key mechanisms that control SW in WAAM components. The re-melting mode ensures wider and deeper molten pool deposition, occasioned by the low layer height (LH) and low WFS, which leads to low SW. The wetting plus spreading mode ensures narrow

and shallow molten pool deposition on the un-melted region, occasioned by high LH and WFS, which leads to high SW [19]. Various mathematical models were developed by Reeves for fused deposition modelling [20], and Luis Perez et al. developed a theoretical model to predict surface roughness [21]. Geng et al. also developed a theoretical model for determining the theoretical value of the molten pool to be inputted to ensure that the WAAM molten metal spread uniformly to cover all un-melted regions to reduce the SW [19]. Other techniques were also developed to control SW using LH and interpass cooling [22]. Xiong et al. also worked on the effect of process parameters to control SW [14].

All the proposed techniques and studies on improving the SW of WAAM components were only able to minimise but not eliminate the entire effects. SW, which acts as a stress raiser, reducing the tensile and fatigue life properties of as-deposited WAAM component, is still a major concern to the industry. The process parameter method of reducing SW is limited with a low deposition rate, and this limits the entire purpose of using WAAM as a low-cost AM process. To fully harmonise and harness the full benefits of the WAAM process, there should be a compromise between SW, productivity and machining and mechanical properties. Gains from high productivity should cover the machining cost and create a break-even point for the industry. The high cost of jigs and features for machining, coupled with the cost of cutting tools, is also limiting the use of machining as a support to the high productivity advantage of WAAM – hence the need for a competitive cold working process that will enhance the SW reduction while maintaining the high productivity level.

Compared to the peening process, rolling is more effective in reducing SW [23] and residual stress in WAAM components [24]. Machine hammer peening (MHP) can only produce beneficial compressive stress to a limited depth below the material surface [25] and will not be suitable for high SW because the largest tools currently available can only achieve up to a few depths of plastic deformation (1.2 mm) into the WAAM surface [26]. Although a novel approach of using MHP to complement rolling in areas of intersections where the rolling rams cannot run is another good method for WAAM SW reduction [26] [10]. This process is currently being developed at Cranfield University as a hybrid WAAM deposition process using two robots. Cold rolling was carried out by Colegrove et al. on a steel WAAM using the profiled and slotted roller to investigate the reduction in residual stresses and distortion observed in welding with their impact on microstructure [23]. Xie et al. also carried out hot rolling (simultaneous deposition and rolling) using a flat roller to improve the geometrical accuracy of 304 stainless steel [8]. Rolling reduced the post-machining time and subsequently enhanced the fatigue properties of the as-deposited structure.

To the best knowledge of the authors, there is no current work showing the effects of using compressive stresses (rolling) to reduce the SW of as-deposited WAAM steel components and how this affects their static and fatigue properties when used in the as-deposited condition. In this study, WAAM of mild steel was carried out using the hybrid process. The effect of compressive residual stress on the mechanical and fatigue properties of the as-deposited component was evaluated. The results for the WAAM as-deposited and WAAM rolled conditions have been compared concerning mechanical strength, fatigue life and fracture behaviour; a correlation with their microstructural variation was also made. Findings from this work show that WAAM as-deposited mild steel components could be used in the as-deposited condition for engineering application with rolling combined to reduce SW.

## 2. Experimental methods

### 2.1 WAAM deposit enhanced by surface rolling

ER70S-6 WAAM structural steel was deposited with dimensions of 245 mm X 120 mm X 5.0 mm and SW of 0.18 mm with the standard cold metal transfer (CMT) welding process using Fronius CMT (VR 7000 CMT) power source. Both sides of the deposited walls were rolled with a constant travelling (TS) of 500mm/min parallel to the welding direction (X-direction) with different loads for different samples (50, 75, 100, 140 and 160 kN) respectively, using a small flat roller with an effective width of 20 mm and a diameter of 120 mm as shown in Fig. 1 (a). The set-up and testing rig are shown in Fig. 1 (b & c). The wire composition and deposition parameters are shown in Tables 1 and 2.

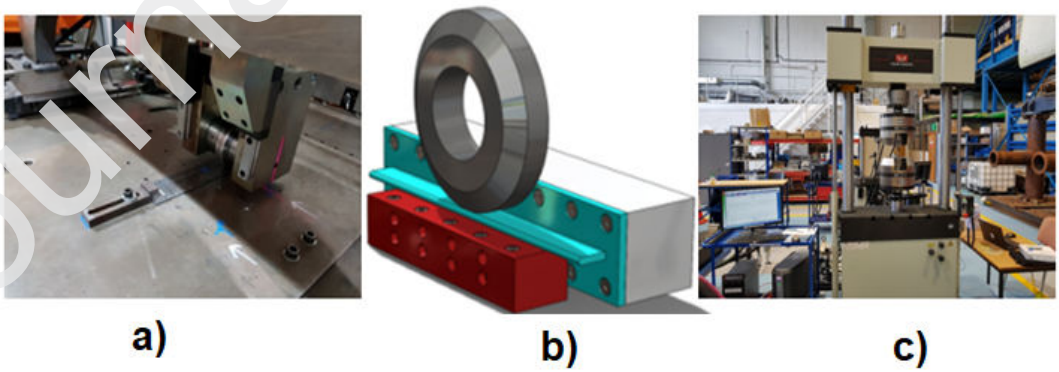


Fig. 1. (a) Set-up (b) roller configuration (c) fatigue testing rig

Table 1. Chemical Composition of Wire

| Chemical Composition (wt %) | | | | | | | | | | | |
|---|---|---|---|---|---|---|---|---|---|---|---|
| Alloys | C | Si | Mn | P | S | Cr | Mo | Ni | Cu | Ti | Zr |
| ER70S-6 | 0.06 | 0.94 | 1.64 | 0.013 | 0.016 | 0.020 | 0.005 | 0.020 | 0.020 | 0.004 | 0.002 |

Table 2. WAAM Deposition Parameters

| Parameters | Values |
|---|---|
| CTWD | 11.5 mm |
| Wire diameter | 1.0 mm |
| Shielding gas | 80% Ar + 20% $CO_2$ |
| Flow rate | 15 L/min |
| WFS | 4.0 m/min |
| TS | 0.4 m/min |
| WFS/TS | 10 |
| Layer height (LH) | 1.6 mm |

## 2.2 Surface waviness, microstructure and hardness characterisation

The WAAM as-deposited structure and the rolled condition samples were transversely cross-sectioned from the wall for metallographic analysis and micro-hardness measurement with the subsequent procedure consisting of grinding polishing and etching in 5% Nital. Micro and macro images of the etched surface were obtained using the optical microscope (Meiji Japan) and deployed to the Axio vision software to reveal the SW parameters (effective wall width, total wall width, notch radius and depth). The micro-hardness was measured by the Zwick/Roell hardness tester across the through thickness direction under a load of 0.2 kg with 10 s holding time. Scanning Electron Microscope ('Philips' SEM) was used to characterise the microstructure and fracture surfaces. The X-ray diffraction (XRD) patterns of WAAM as-deposited (70 -A) and WAAM as-deposited + rolled (160 KN) was measured on a D8 Advance X-ray diffractometer (Bruker AXS, USA) using a Lynxeye detector and Cu $K_\alpha$ radiation, with wavelength $\lambda = 0.154$ nm, 30 kV, and 10 mA. The scanning angle was between 10˚ and 90˚, at a scanning speed of 10˚/min, and a step size of 0.02˚/s.

## 2.3 Mechanical characterisation

All tests were done at ambient temperature. The tensile test was performed in accordance with ASTM E8/E8M-16a on all tensile samples, as given in Table 3. A gauge length of 32 mm was used to calculate the elongation. A strain rate of 1mm/min was utilised. The uni-axial tensile testing was performed with a 100 kN electromechanical controlled INSTRON 5500R machine with a load cell of 30 kN

Table 3. Tensile samples

| Tensile sample condition | Surface waviness(mm) | Number of samples |
|---|---|---|
| As-deposited | 0.18 | 3 |
| Machined | N/A | 3 |
| As-deposited + rolled | 0.08, 0.13, 0.17 | 9 |
| As-deposited +rolled + Machined | N/A | 3 |

Table 4. Fatigue samples

| Fatigue sample condition | Surface waviness(mm) | Number of samples |
|---|---|---|
| As-deposited | 0.18 | 5 |
| Machined | N/A | 6 |
| As-deposited + rolled | 0.08 | 3 |

The fatigue test was performed in accordance with ASTM E466-15 on all fatigue samples, as given in Table 4. A tension-tension fatigue test was carried out with a frequency of 10 Hz and a stress ratio of R = 0.1 using an Instron machine equipped with a 250 KN load cell. The fatigue response of the different conditions was established at different stress levels to build an S-N curve. The test programme was set up to compare the mechanical properties between the three fatigue sample conditions as detailed in Table 4. These samples will be subjected to the same loading condition in service. The WAAM build structure showing the build direction and the welding direction is shown in Fig. 2(a). The dimensioning of the fatigue specimen and the tensile specimen is shown in Fig. 2 (b & c).

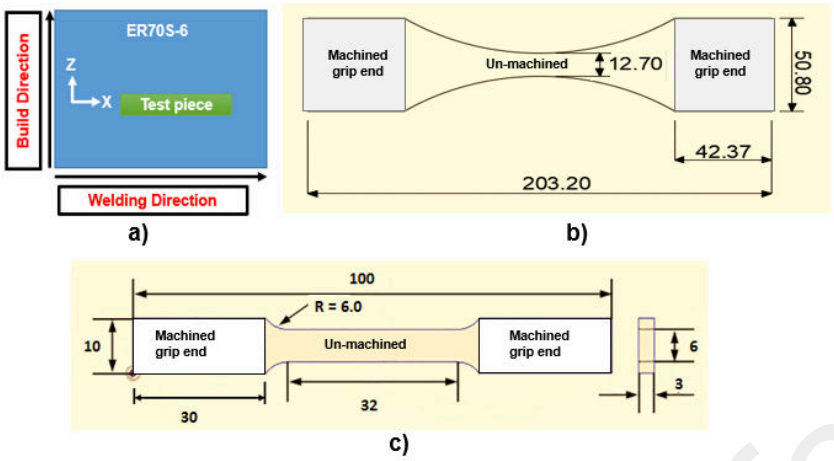


Fig. 2. (a) Build orientation (b) fatigue testing geometry (c) tensile testing geometry

## 3. Results

### 3.1. Surface waviness and stress concentration factors (as-deposited & rolled)

The WAAM build and specimen loading direction is shown in Fig. 3 and Fig. 4 and presents the variation in SW and stress concentration factor (SCF) of both conditions and the relationship between rolling load P and SW. The macrostructure showing the effect of the rolling load on WAAM as-deposited is shown in Fig. 5. The measured SW of the rolled WAAM samples, as shown in Fig. 4, revealed that the SW decreases with the increase in the rolling load. The measured SW of the as-deposited WAAM sample was 0.18 mm without rolling; this further reduces to 0.08 mm with a rolling load of 160 kN. It is also evident that the total wall width (TWW) as shown in Fig. 3 (d) also decreases as the SW decreases, as shown in Fig. 5 (b-d). The peaks of the as-deposited samples are reduced as the rolling load increases because of plastic deformation.

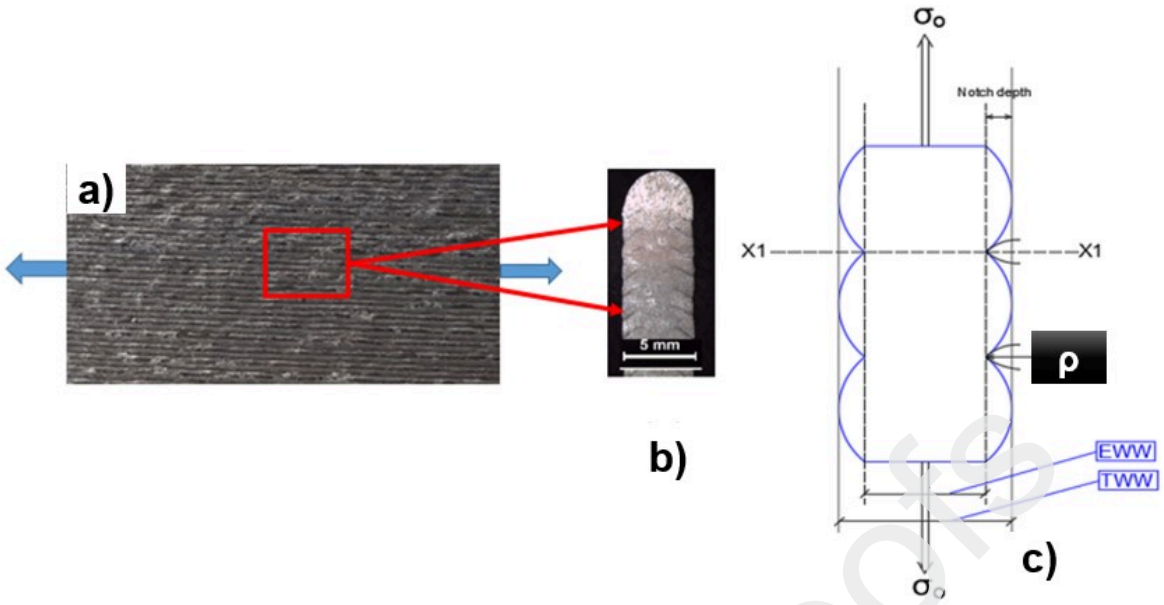


Fig. 3.(a) as-deposited WAAM loading in welding direction (X-direction) (b) etched cross-section of as-deposited WAAM (c) as-deposited schematic illustrating SW parameters and notch depth

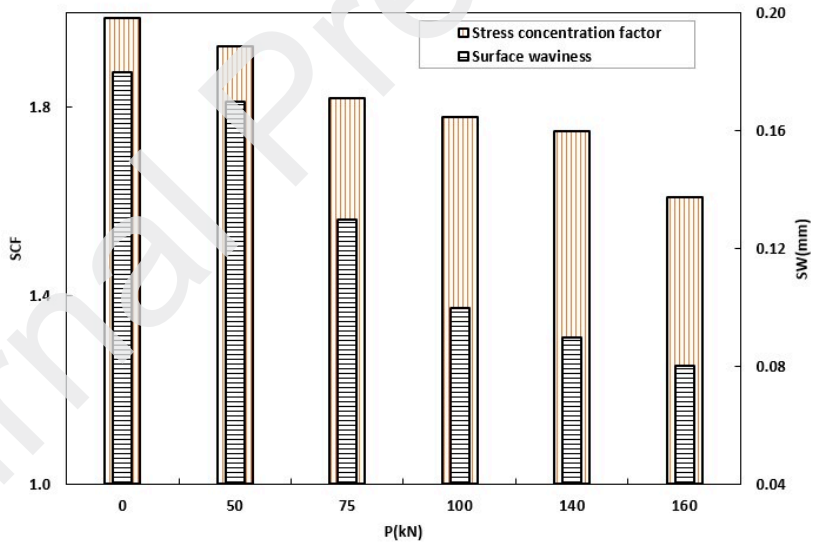


Fig. 4. Variation in SCF and SW of WAAM as-deposited and rolled conditions of ER70S-6

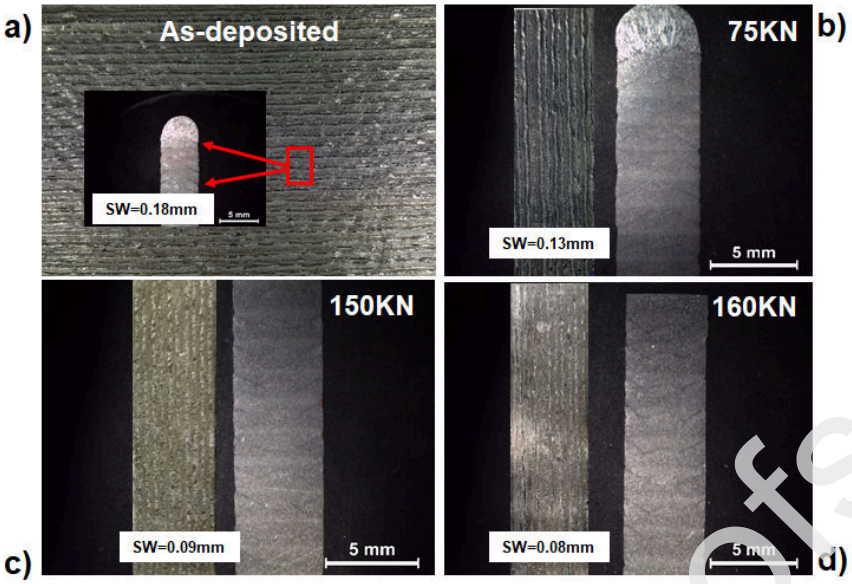


Fig. 5. Macros showing the effects of rolling load on WAAM as-deposited

### 3.2. Monotonic properties - tensile strength

Fig. 6 presents the stress-strain curve obtained from the tensile samples in Table 3. The tensile strength (ultimate tensile strength, UTS and yield strength, YS) are on the increase as the rolling load increases. It is important to note that the as-deposited condition with SW of 0.18mm yielded the least strength values. The as-deposited + rolled + machined condition without any SW showed the highest tensile strength, with the least percentage elongation (PCE) as shown in Fig. 6, it is evident that SW reduces the tensile strength. The interrupted yielding phenomenon called the luder band elongation tends to disappear due to work-hardening rate effects incurred from the plastic deformation process [27,28]. This interrupted yielding decreases with the rolling loading as seen in Fig. 6. The as-deposited + machined condition showed higher PCE compared to the as-deposited + rolled. The interaction plot for rolling load versus UTS and SW is shown in Fig. 7.

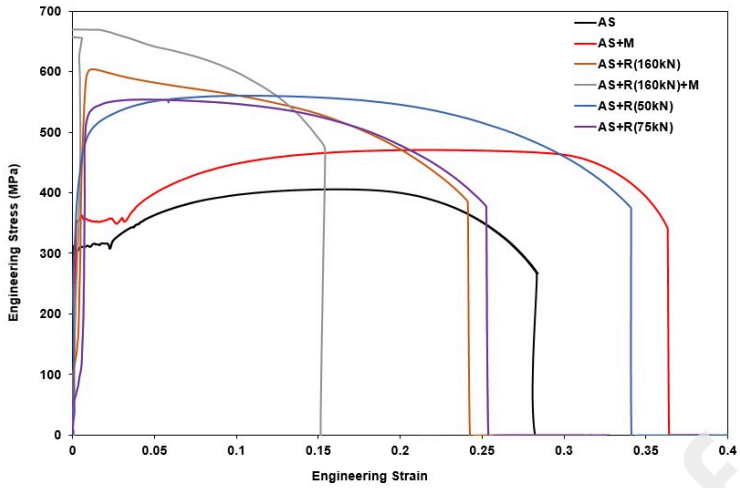


**Fig. 6.** Stress-Strain curve of the various conditions of WAAM ER70S-6

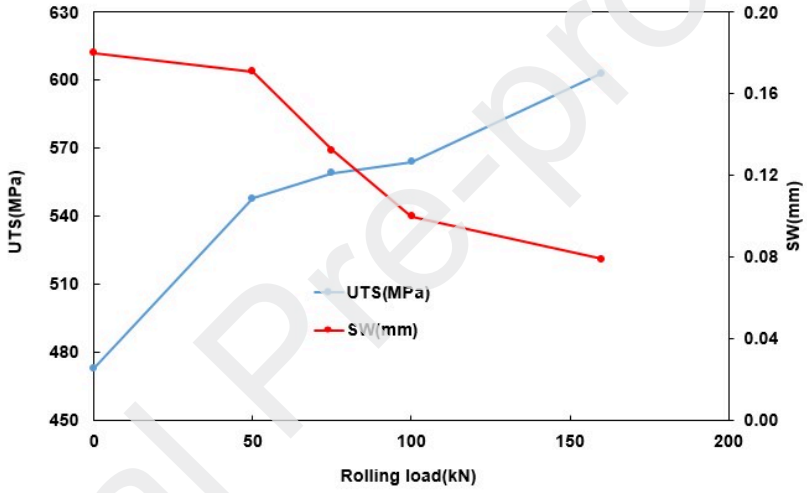


**Fig. 7.** Interaction plot for rolling load P(KN) versus UTS and SW

## 3.3. Hardness profile and microstructural variation

The hardness versus depth plots across the through thickness direction for both as-deposited and the various rolled conditions are shown in Fig. 8. The SEM images showing the effect of rolling on the microstructure are shown in Fig. 9. The average hardness of the as-deposited + rolled increases with the rolling load. The 160 kN samples show the maximum hardness of 233 ± 1.5 HV at both rolled surfaces, while the 50 and 75 kN samples show maximum hardness of 225 ± 1.0 & 219 ± 1.5 HV at both rolled surfaces, respectively. Both as-deposited + rolled conditions showed minimum hardness at the midpoint of the sample. The as-deposited condition showed a

maximum hardness of 186 ± 2.0 HV, which is 25.26% lower than the maximum obtained hardness obtained with 160 KN rolled condition. The increase in hardness with the rolling load is a result of more dislocation density being generated by the higher rolling load, which work-harden the material [29], and as a result of the stacking fault energy [30],[31]. In Fig. 9, the as-deposited (Fig. 9 (a)) has a grain size of 14.5μm, which is bigger than the as-deposited + rolled (Fig. 9 (b-d)), which had grain sizes decreasing as the rolling load increased. The 160 kN sample had elongated grains with a size of 8.6μm. Rolling plastically deforms the surface and re-distribute the grains due to the increase in dislocation density. It has also been reported that it caused austenite nucleation and provided further grain size reduction [23]. In these studies rolling plastically deforms the peaks of the SW, shown in Fig. 3 (c), into surfaces, shown in Fig. 5 (b-d), hence reducing the TWW and the SW as well. This is also in support of the claim by Colegrove et al. [23] and Hönnige et al. [29]. The plastic deformation induced on the surface, which is a function of the rolling load reduces not only SW but also the residual stress. This has been proved to improve the mechanical properties of the WAAM deposit.

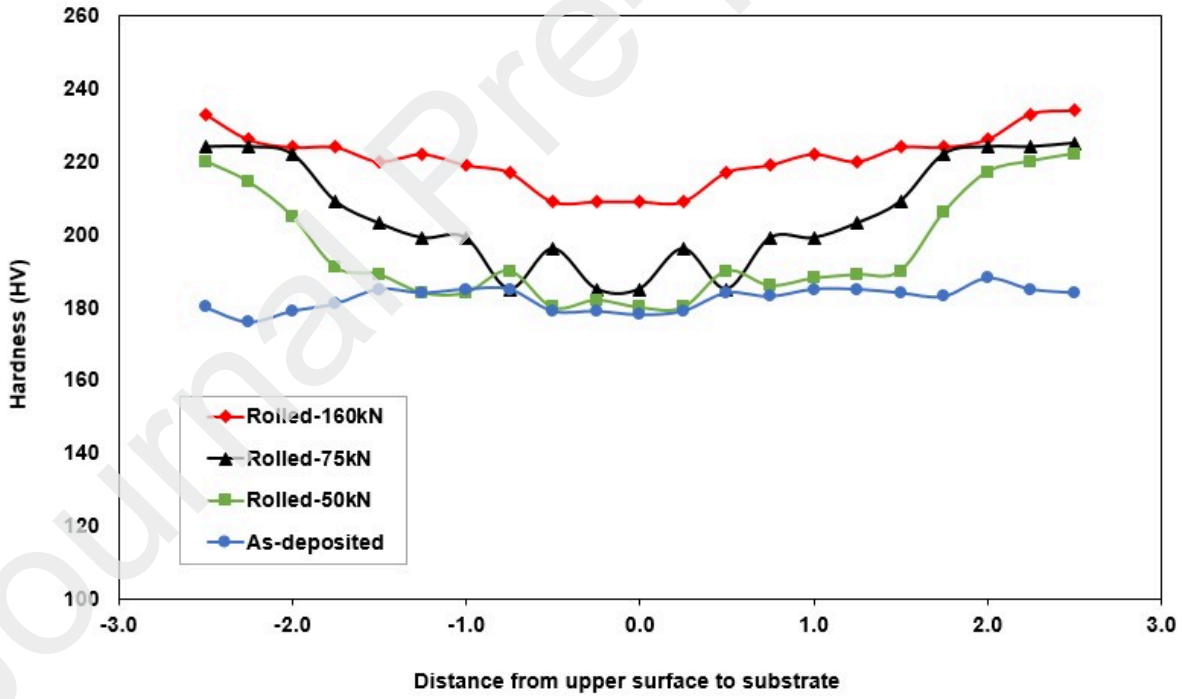


**Fig. 8**. Effect of rolling load P(kN) and hardness variation across the through thickness direction (rolling on both surfaces)

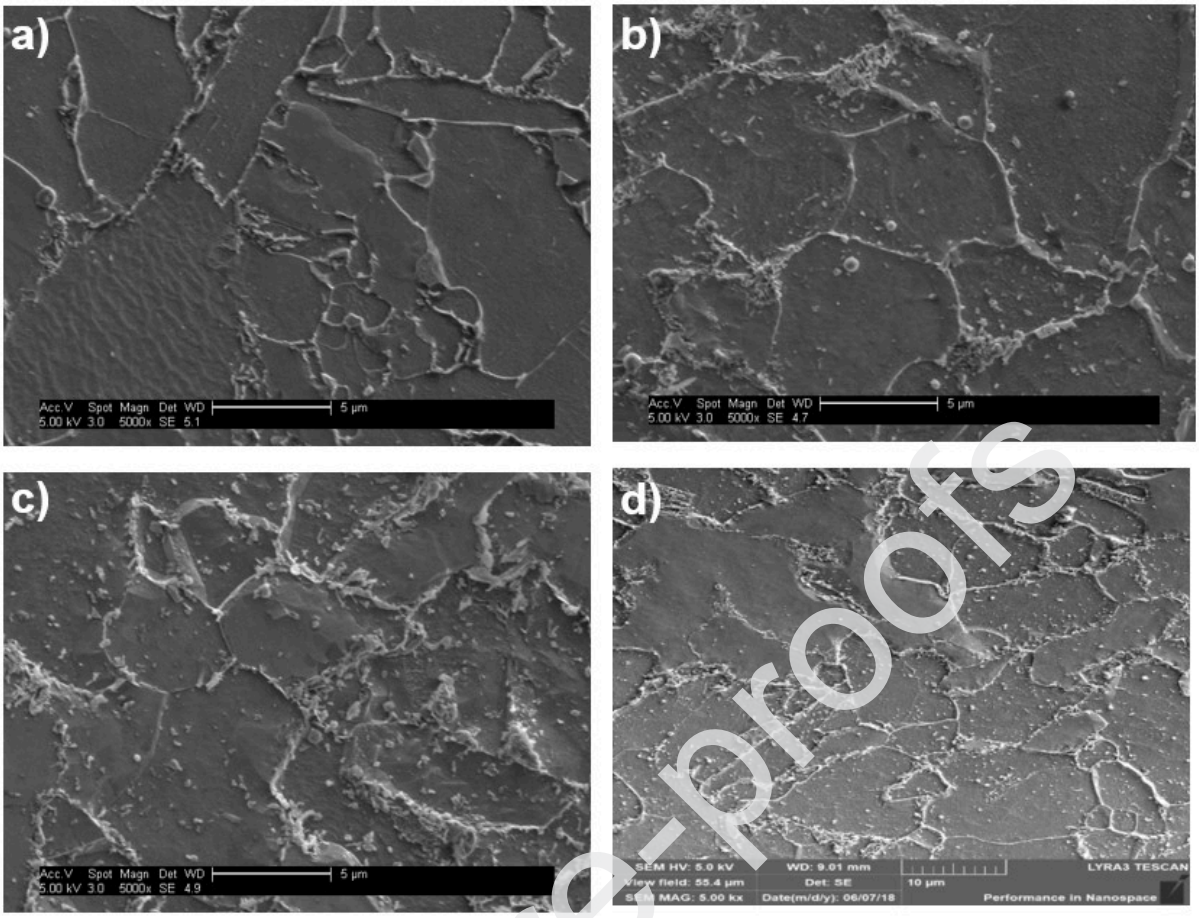


Fig. 9. SEM images (a) as-deposited (b) as-deposited + rolled (50 kN) (c ) as-deposited + rolled (75 kN) (d) as-deposited + 160 kN

## 4.0 Discussion

### 4.1 Macroscopic failure mechanism of as-deposited and rolled WAAM structures

The effect of notch radius on SW for both rolled, and the as-deposited condition is presented in Fig. 10 (a) while Fig. 10 (b) presents the effect of the SCF on the SW of both rolled and as-deposited condition. It is evident from this study that the notch radius, (**ρ**) (as indicated in Fig. 3 (c)), increases as the SW reduces (Fig. 10 (a)). Low values of SW give rise to a corresponding increase in notch radius, as shown in Fig. 10 (a). Rolling reduces the notch depth (as indicated in Fig. 3 (d)) and increases the notch radius. Smaller notch radius (0.2mm) as seen in Fig. 10 (a) is as a result of high SW (0.32mm), which consequently leads to a high SCF of 2.48, as shown in Fig. 10 (b). This is observed in the as-deposited condition. Larger notch radius (0.68 mm) as seen in Fig. 10 (a) is as a result of low SW (0.09 mm), which consequently leads to a low SCF of 1.65, as shown in Fig. 10 (b). This is

observed in the rolled condition. The rolled condition shows a smooth transition between the layers, as shown in Fig. 5 (b-d), while the as-deposited condition shows a sharp transition between layers, hence served as points of high-stress concentrations. Failure in WAAM as-deposited is always from this point of weakness.

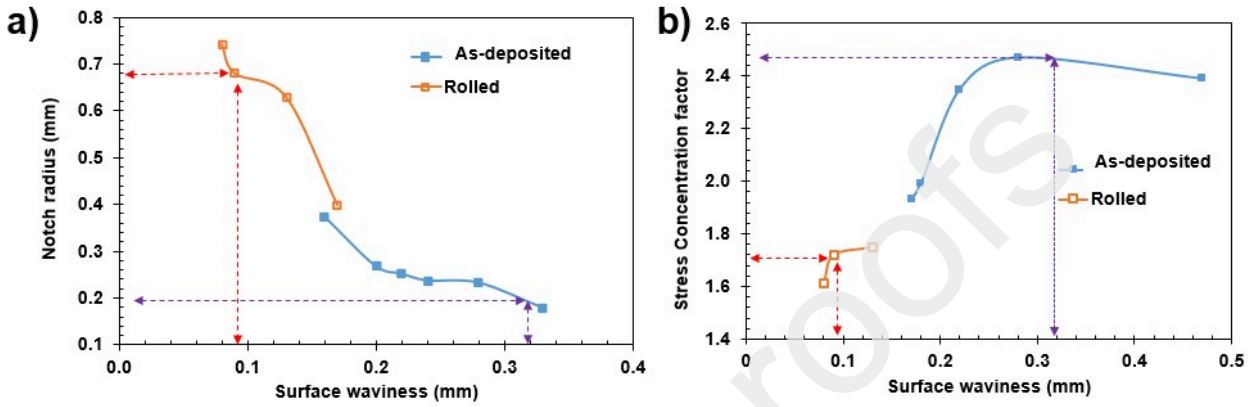


Fig. 10. Parameters effects (a) effect of notch radius on SW for both rolled and as-deposited condition (b) effect of SCF on SW of both rolled and as-deposited condition

## 4.2 Tensile fractures modes and morphologies

Table 5 shows the average static tensile test values of WAAM as-deposited, machined and rolled under different conditions. The tensile fracture morphology in the various conditions is presented in Fig. 11. It is evident from the results that the UTS and YS are in direct correlation with the level of SW. High SW leads to reduced tensile properties. The SW serves as points of fracture initiation – the higher the SW, the quicker to failure the sample will be. It is evident from Table 5 that the application of rolling which reduces the SW. as seen in Fig. 10 (a & b), also enhanced the UTS and YS of the WAAM deposit. Rolling with 160 kN force produced a 55% and 49.25% enhancement on the SW and UTS respectively. While a rolling load of 75 kN produce 27% and 3.9% in SW and UTS enhancement respectively. But PCE, on the other hand, is decreased as the rolling load increased. There was a decrease of 37% in the PCE when a rolled load of 160 kN was applied to the as-deposited condition. Rolling induced strain effects that reduced the thickness and increased the length in the rolled direction as a result of plastic flow [29]. The machined condition without SW showed higher UTS and YS compared to the as-deposited condition. The as-deposited + rolled + machined condition produce a UTS and YS of 665 MPa and 608 MPa

respectively, but with the lowest PCE of 15%, hence rolling enhanced, microstructural changes are responsible for these properties.

**Table 5**. Average static tensile test values of WAAM(ER70S-6) as-deposited, as-deposited + rolled and as-deposited + machined

| P-(kN) | SW(mm) | SCF | UTS(MPa) | $YS,Rp_{0.2}$(MPa) | Elongation(%) | Condition |
|---|---|---|---|---|---|---|
| 0 | 0.18 | 1.99 | 402 ± 2.0 | 300 ± 1.5 | 30 ± 1 | As-deposited |
| 160 | 0.08 | 1.61 | 600 ± 3.0 | 574 ± 2.6 | 22 ± 2 | As-deposited + Rolling |
| 75 | 0.13 | 1.82 | 552 ± 1.0 | 498 ± 5.0 | 23 ± 2 | As-deposited + Rolling |
| 50 | 0.17 | 1.93 | 546 ± 3.0 | 486 ± 2.6 | 32 ± 2 | As-deposited + Rolling |
| - | - | - | 470 ± 2.0 | 350 ± 1.5 | 35 ± 3 | As-deposited + Machined |
| - | - | - | 665 ± 2.0 | 608 ± 1.5 | 15 ± 3 | As-deposited + Rolled + Machined |

The fracture morphology of the as-deposited as seen in Fig. 11 (a) is characterised by conical equiaxed dimples formed from microvoid coalescence rupture, indicating a high level of ductile tearing with low strength. Precipitates in the form of inclusions are also seen. The dimples in the as-deposited are more oval and ductile compared to the as-deposited + rolled condition. The as-deposited + rolled + machined condition as seen in Fig. 11 (b) has smaller and deeper dimples, hence the higher strength with reducing ductility. The as-deposited + rolled condition as showed in Fig. 11 (c) is dominated by a mixture of large and small elongated dimples as a result of rolling, enhancing the elongation of the grain structure as a result of plastic deformation. Hence the shear elongated dimples lead to high UTS and YS, with reduced ductility compared to the as-deposited condition.

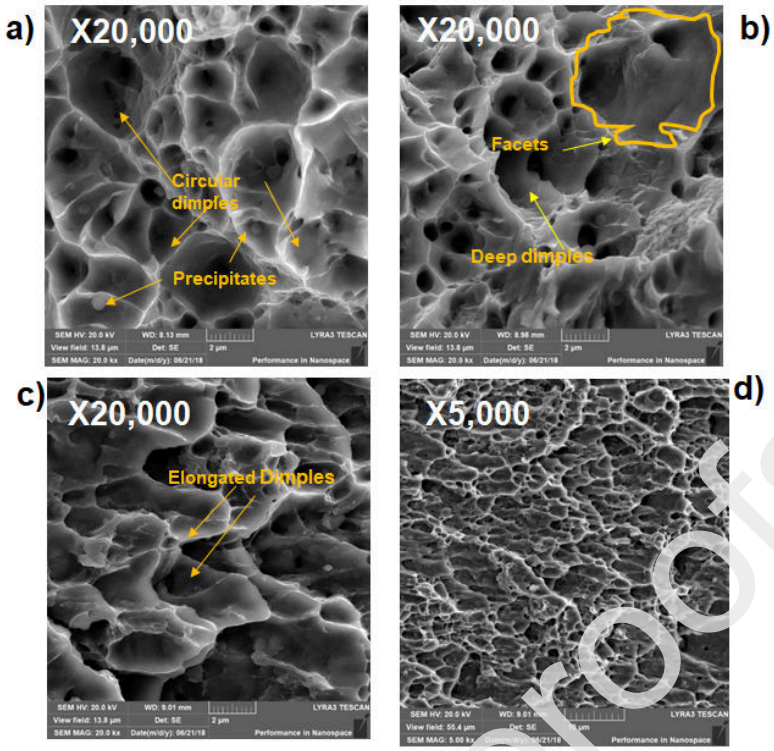


**Fig. 11.** Tensile fracture morphology of WAAM ER70S-6 (a) as-deposited (b) as-deposited + rolled (160 kN) + machined (c) as-deposited + rolled (160 kN(X20, 000)) (d) as-deposited + rolled (160 kN(X5, 000))

### 4.3 Rolling enhanced microstructural changes

The XRD patterns of the as-deposited (70-A) and rolled (160 kN) are shown in Fig. 12 (a). Only the martensite phase was observed in both samples with no appearance of the austenite phase, i.e. no phase transformation after the sample was subjected to rolling. At diffraction angles (2Θ) of 45.18°, 65.31° and 82.71°, the samples exhibit peaks on Fe (110), Fe (200), Fe (211) planes, whereas a little broadening of the peaks on all the three planes is observed for the rolled sample (Fig. 12 (b-d)). The broadening of the peaks experienced by the rolling sample could be ascribed to the structural refinement in the orientation of the sample. The rolled sample (160 kN) experienced a higher intensity in the XRD pattern as compared to the as-deposited. Using Scherrer's equation, the volume of the phases was calculated to be 0.02263 $nm^3$, 0.02322 $nm^3$, and 0.02326 $nm^3$, for the (110), (200), and (211) phases, respectively. Due to the peak broadening, as shown in the XRD analysis (Fig. 12) and structural refinement in orientation observed in the rolled-160 kN sample, compressive residual stress was induced which increases the volume fraction of the martensite. Compared to the as-deposited sample, the volume fraction of the martensite phase in the rolled-160 kN sample increases as the rolling time increases, thereby strengthening the

sample through plastic deformation and increasing the hardness in the process. This could be responsible for the high hardness experienced by the rolled-160 kN sample in Fig. 8. Furthermore, the volume fraction of the martensite phase of the rolled-160 kN sample, which is strongly dependent on the level of deformation induced from the rolling process, increases with the rolling load. This increases the stacking-fault energy originating from the deformation process, thereby improving the hardness of the rolled condition and hence enhancing the strength and fatigue life.

Fig. 13 shows the transmission electron microscope (TEM) images of the as-deposited and rolled (160 kN) WAAM steel. In the as-deposited condition, Fig. 13 (a-c), thin like-shaped cementite particles are observed inside the lath with increased dislocation density of the cementite; besides, lath martensite was produced. Dislocation at the lath boundaries was also produced with sub-grain boundaries (nanoscale) or prior austenite grain boundaries (Fig. 13 (c)). Furthermore, a well-developed dislocation substructure is observed in the volume of martensite crystals in the as-deposited samples. The thin lath-like particles of cementite appeared in the martensite laths by the beginning of deformation (Fig. 13 (a-c)). The TEM images in Fig. 13 (d & e) reveal the production of grains which were separated by high-angle grain boundaries (HAGBs). Most of the grains in the rolled samples are heavily strained and contain a high density of dislocations, as indicated in Fig. 13 (d & e).

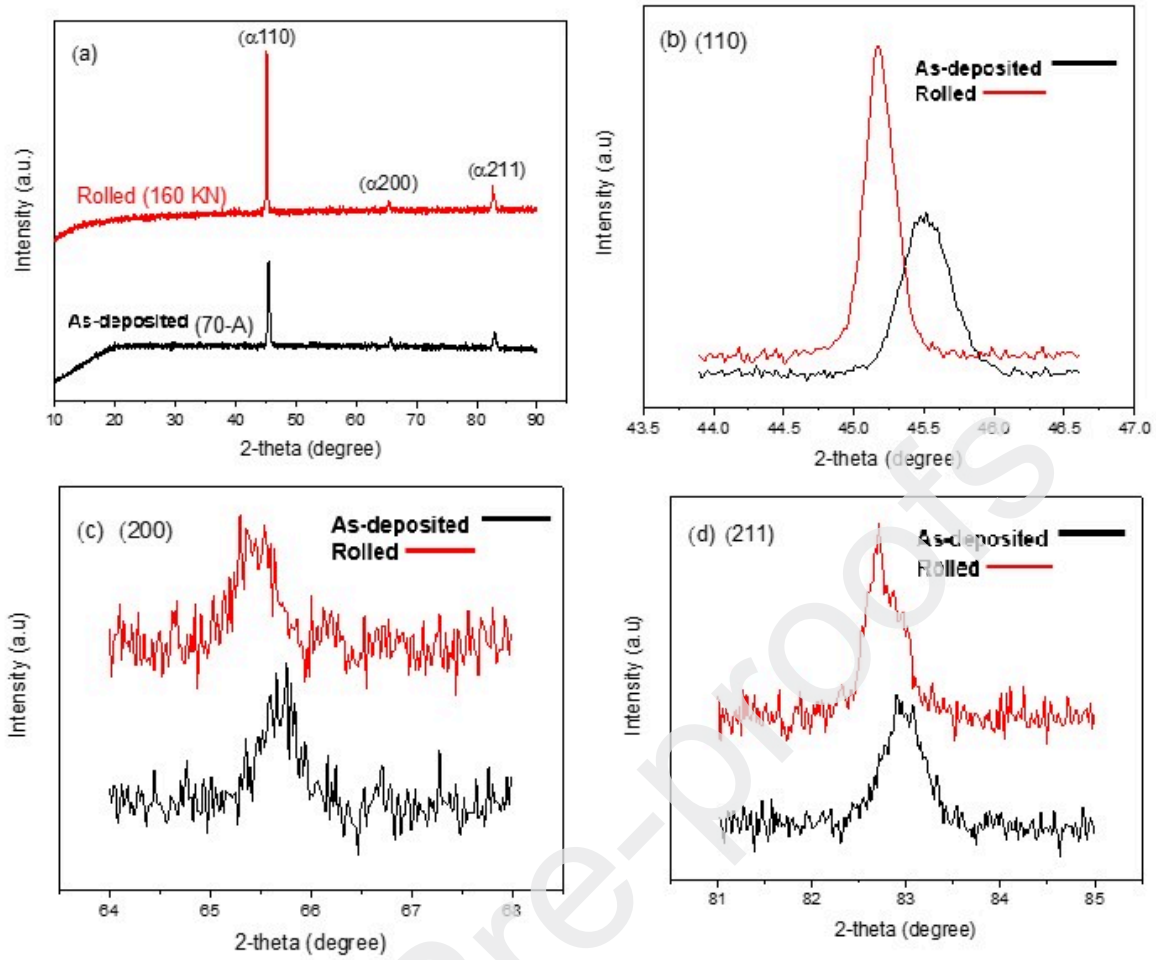


Fig. 12. XRD Pattern of untreated (70-A) and treated (160 kN) mild steel (a); detailed XRD patterns for the peaks: Fe (110) (b), Fe (200) (c), Fe (211) (d)

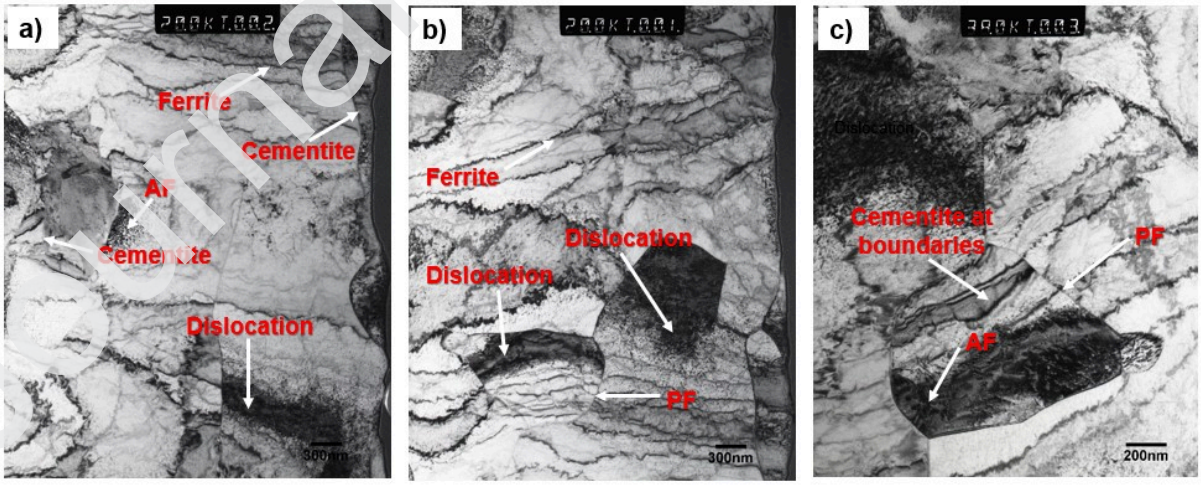

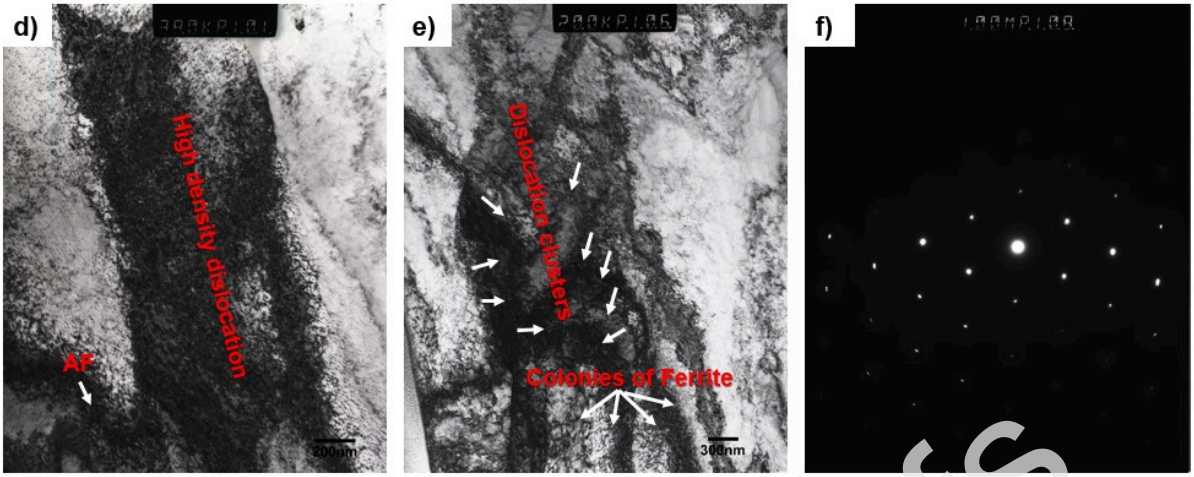


Fig. 13. TEM image of; as-deposited (a-c) samples and as-deposited + rolled (160 kN) (d-f)

### 4.4. Fatigue responses and microscopic failure mechanism

The high cycle fatigue behaviour of the WAAM as-deposited, machined and as-deposited + rolled is displayed in Fig. 14. The as-deposited condition has a SW of 0.18 mm (180 µm), while the as-deposited + rolled condition has an SW of 0.08 mm (80 µm) when rolled with a force of 160 kN. The machined condition showed better fatigue limit than other conditions. But, generally, rolling improved the fatigue limit of the as-deposited samples. Fig. 15 presents the fractography of WAAM ER70S-6 in the machined condition, Fig. 16 also shows the fractography of the as-deposited condition, while the fractography analysis of the as-deposited + rolled condition is displayed in Fig. 17.

Crack initiation mechanism and failure path in the machined condition is essentially by a ductile fracture through microvoid coalescence from the weakened path formed by the hard spots at the surface of the machined samples during fatigue testing, as shown in Fig. 15 (a). Silicon and manganese oxides inclusions are formed as a result of the oxidising potential of the shielding gas used for the deposition, and the relatively high heating and rapid cooling of the WAAM process [32]. These inclusions serve as hard spots with high-stress concentrations and areas of quick failure initiation for the machined condition as the effect of SW has been eliminated by machining [33]. Fatigue crack growth is through ductile striations caused by cyclic hardening as a result of crack tip blunting by slip during loading and unloading. The ductility of this material also supports the fatigue crack growth behaviour, as shown in Fig. 15 (b & c). The striation spacing is closer than the observation in the as-deposited condition, as

shown in Fig. 16 (a & b), hence a higher fatigue life of 107,698 cycles at maximum stress of 492MPa. The main function of the added micro-alloying (Ti, Cu & Zr) as shown in Table 1. is for precipitation strengthening. And the promotion of acicular ferrite formation, which induces microstructural refinement [34] – hence the behaviour of the material.

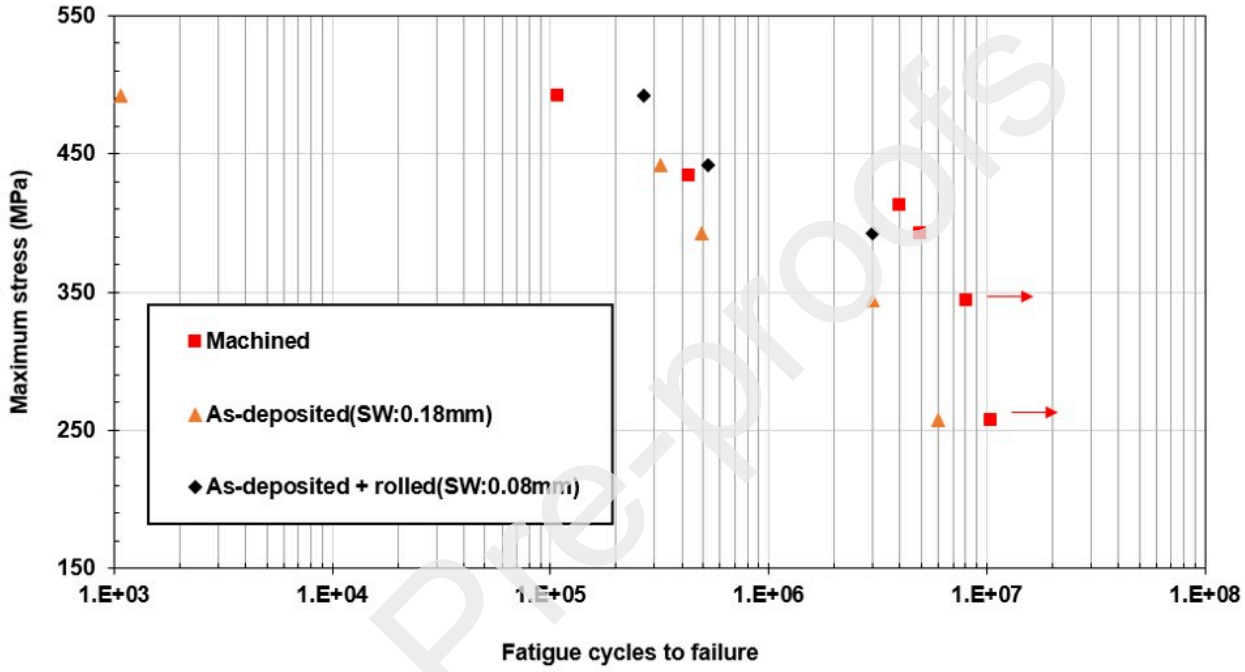


Fig. 14. High cycle fatigue properties (R=0.1) of WAAM ER70S-6 in the as-deposited, as-deposited + rolled and machined condition

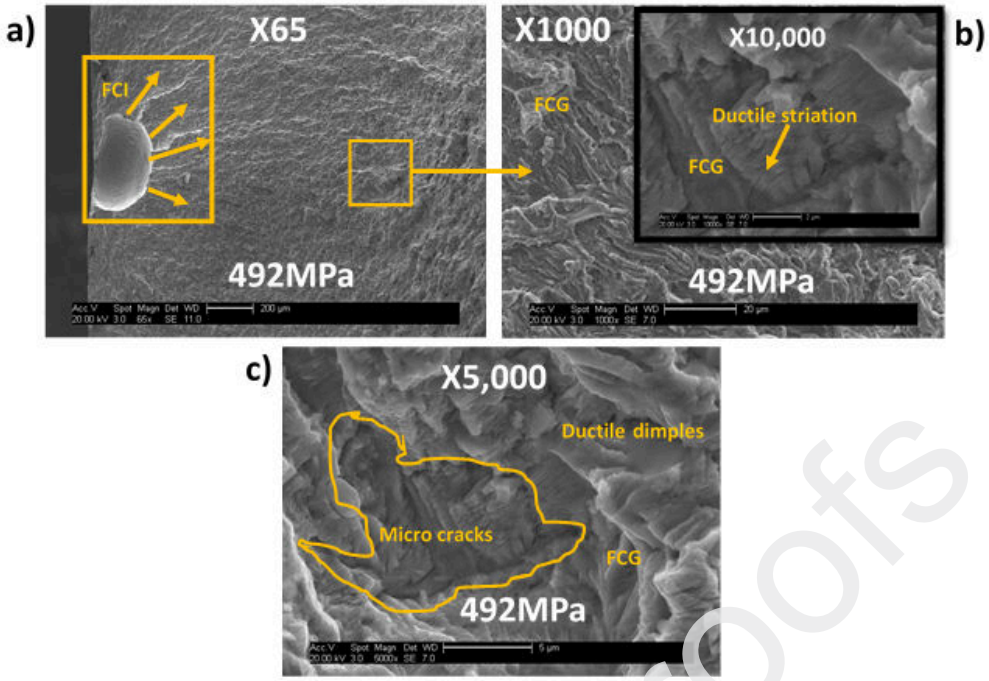


Fig. 15. SEM Fractography of WAAM ER70S-6 in the machined condition, (a-c) $\sigma_{max} = 492MPa$ , $N_f$ = 107,698 cycles

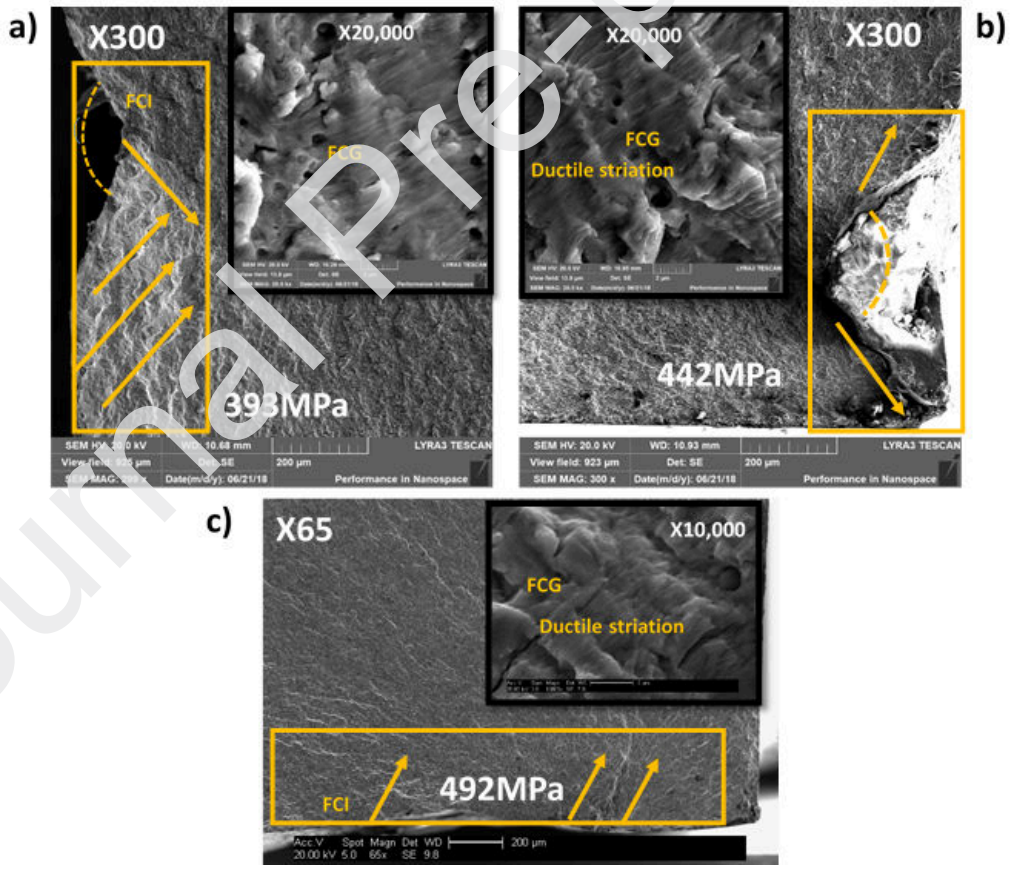


Fig. 16. SEM Fractography of WAAM ER70S-6 (as-deposited) $(a)\sigma_{max} = 393MPa$ , $N_f$ = 495,119 cycles (b), $\sigma_{max} = 442MPa$ , $N_f$ = 318,145 cycles (c),$\sigma_{max} = 492MPa$ , $N_f$ = 1,069 cycles

The significant reduction in fatigue life for the as-deposited sample is primarily due to the presence of notches (surface waviness) which act as stress raisers. The cracks initiated at the trough (pit) of the SW and propagated towards the centre of the specimen, at a critical length, where the remaining sample ligament could no longer support the increasing stress level, a plastic collapse will occur. Maximum stress concentration occurs between any two layers that form the SW profile, as shown in Fig. 16 (a). Increasing the notch radius and decreasing the depths of the SW with plastic deformation (rolling), relaxes the stress concentration effects. The lower the SCF of the WAAM as-deposited surface, the more useful it becomes if the application were monotonic, or cyclic loading is involved. Initiation of cracks during fatigue loding is normally from the outside and propagating inward till failure, as shown in Fig. 16 (b). The fractography also reveals multiple crack initiation sites at the surface, independently of the stress amplitude condition. The closer the included angle between layers to 180°, as shown in Fig. 16 (a & b), the greater the resistance to fatigue crack failure. The fatigue response of the WAAM as-deposited part is largely determined by the WAAM deposition parameters and build sequence. The fractography shows that the striation spacing is dependent on the stress level applied to the as-deposited condition. The lower fatigue life of 1,069 cycles at maximum stress of 492MPa was also observed with the as-deposited condition as a result of the effect of SW.

The crack initiation site and path in the as-deposited + rolled WAAM surfaces is from the weakened valley with the maximum stress concentration between two layers where their curvature was not effectively reduced, as shown Fig. 17 (a & c). The notch radius is increased by the rolling force, as shown in Fig. 17 (a) where the depth between two layers is reduced, hence the reduction of the SCF on the rolled surface. The higher the load, the lower the SW, as shown in Fig. 4. The as-deposited + rolled had a life improvement of 66% at a stress level of 442MPa as compared to the as-deposited condition. The as-deposited + rolled showed a higher fatigue life (266,856 cycles) at a stress level of 492MPa, higher than the as-deposited condition (1,069 cycles) and the machined condition (107,698 cycles). Most of the grains in the rolled samples are heavily strained and contain a high density of dislocations, as indicated in Fig. 13 (a & b), hence an improvement in fatigue life.

Rolling improves the usefulness of the WAAM as-deposited part by plastically deforming the peaks of the SW, hence increasing notch radius and decreasing the depths which are points of the stress raiser. The deformed notches and valleys are responsible for delaying the initiation of cracks when subject to static and dynamic loading. It has also been reported that compressive stress from rolling also retards crack propagation in a structure [35].

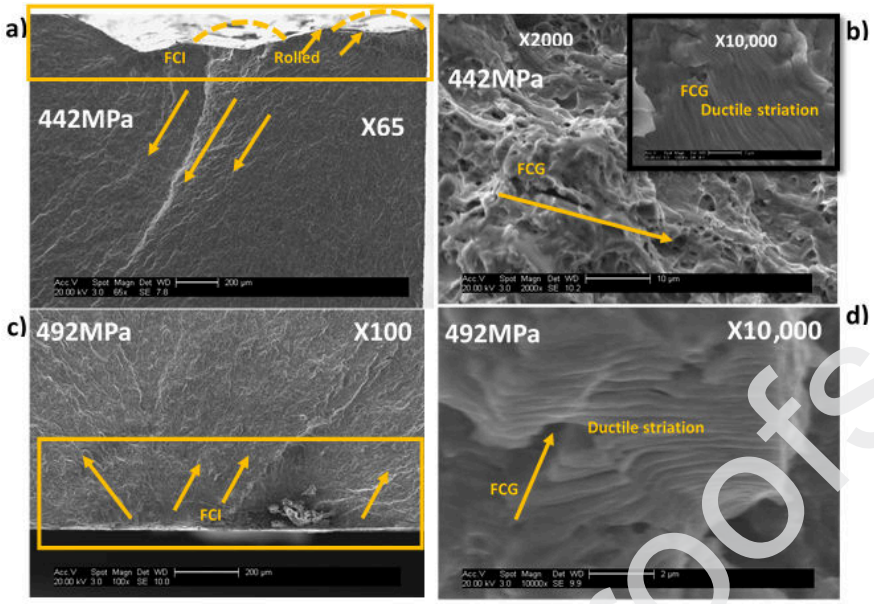


Fig. 17. SEM Fractography of WAAM ER70S-6 (as-deposited + rolled_160KN) (a-b)$\sigma_{max} = 442MPa$ , $N_f =$ 530,319 cycles (c-d) $\sigma_{max} = 492MPa$ , $N_f = 266{,}856$ cycles (c)

## 5. Conclusions

In this study, the functionality of WAAM mild steel in the as-deposited condition was enhanced by rolling to improve its surface finish and fatigue life.

- High SW is detrimental to the mechanical strength and fatigue life of an as-deposited WAAM steel structure.
- Compressive stress induced by rolling on the as-deposited condition reduces the SW and produces an increase in mechanical and fatigue strength due to the macroscopic and microscopic influence.
- Reduction of the SW is achieved by the increase of the notch radius of the valley between two SWs in WAAM as a result of rolling. Compressive stress induced by rolling and notch radius reduction is responsible for fatigue life improvement.
- WAAM mild steel components could be used in the as-deposited condition for engineering application when rolling is applied to reduce its SW.
- Finally, the failure mechanism for the as-deposited condition is the macroscopic mechanism, whereas the microscopic mechanism is dominant for the machined condition.

**Acknowledgements:**

The authors acknowledge the funding from the European Union's HORIZON 2020 research and innovation programme under grant agreement No 723600. The authors also acknowledge the support of Vestas Wind Systems A/S and Total E & P Nigeria Limited (TEPNG) for their financial support.

**References**

[1] The Crown Estate. Offshore Wind Operational Report January-December. 2018.

[2] The Crown Estate. Offshore Wind Operational Report January-December. 2016.

[3] Thompson MK, Moroni G, Vaneker T, Fadel G, Campbell RI, Gibson I, et al. Design for Additive Manufacturing: Trends, opportunities, considerations, and constraints. CIRP Ann - Manuf Technol 2016;65:737–60. doi:10.1016/j.cirp.2016.05.004.

[4] Lockett H, Ding J, Williams S, Martina F. Design for Wire + Arc Additive Manufacture: design rules and build orientation selection. J Eng Des 2017;4828:1–31. doi:10.1080/09544828.2017.1365826.

[5] Williams SW, Martina F, Addison AC, Ding J, Pardal G, Colegrove P. Wire + Arc Additive Manufacturing. Mater Sci Technol 2016;32:641–7. doi:10.1179/1743284715Y.0000000073.

[6] Xu X, Ganguly S, Ding J, Dirisu P, Martina F, Liu X, et al. Improving mechanical properties of wire plus arc additively manufactured maraging steel through plastic deformation enhanced aging response. Mater Sci Eng A 2019;747. doi:10.1016/j.msea.2018.12.114.

[7] Ding D, Pan Z, Cuiuri D, Li H. Wire-feed additive manufacturing of metal components: technologies, developments and future interests. Int J Adv Manuf Technol 2015;81:465–81. doi:10.1007/s00170-015-7077-3.

[8] Xie Y, Zhang H, Zhou F. Improvement in Geometrical Accuracy and Mechanical Property for Arc-Based Additive Manufacturing Using Metamorphic Rolling Mechanism. J Manuf Sci Eng 2016;138:111002. doi:10.1115/1.4032079.

[9] Martina F, Ding J, Williams S, Caballero A, Pardal G, Quintino L. Tandem Metal Inert Gas process for high productivity Wire Arc Additive Manufacturing in stainless steel. Addit Manuf 2018;25:545–50. doi:10.1016/j.addma.2018.11.022.

[10] Donoghue J, Antonysamy AA, Martina F, Colegrove PA, Williams SW, Prangnell PB. The effectiveness of combining rolling deformation with Wire-Arc Additive Manufacture on β-grain refinement and texture modification in Ti-6Al-4V. Mater Charact 2016;114:103–14. doi:10.1016/j.matchar.2016.02.001.

[11] Brandl E, Schoberth A, Leyens C. Morphology, microstructure, and hardness of titanium (Ti-6Al-4V) blocks deposited by wire-feed additive layer manufacturing (ALM). Mater Sci Eng A 2012;532:295–307. doi:10.1016/j.msea.2011.10.095.

[12] Almeida PMS. Process Control and Development in Wire and Arc Additive Manufacturing 2012:1–467.

[13] Geng H, Li J, Xiong J, Lin X, Huang D, Zhang F. Formation and improvement of surface waviness for additive manufacturing 5A06 aluminium alloy component with GTAW system. Rapid Prototyp J 2018;24:342–50. doi:10.1108/RPJ-04-2016-0064.

[14] Xiong J, Li Y, Li R, Yin Z. Influences of process parameters on surface roughness of multi-layer single-pass thin-walled parts in GMAW-based additive manufacturing. J Mater Process Technol 2018;252:128–36. doi:10.1016/j.jmatprotec.2017.09.020.

[15] Ding J, Colegrove P, Mehnen J, Ganguly S, Almeida PMS, Wang F, et al. Thermo-mechanical analysis of Wire and Arc Additive Layer Manufacturing process on large multi-layer parts. Comput Mater Sci 2011;50:3315–22. doi:10.1016/j.commatsci.2011.06.023.

[16] Michel F, Lockett H, Ding J, Martina F, Marinelli G, Williams S. A modular path planning solution for Wire + Arc Additive Manufacturing. Robot Comput Integr Manuf 2019;60:1–11. doi:10.1016/j.rcim.2019.05.009.

[17] Wang X, Wang A, Li Y. A sequential path-planning methodology for wire and arc additive manufacturing based on a water-pouring rule. Int J Adv Manuf Technol 2019:3813–30. doi:10.1007/s00170-019-03706-1.

[18] Wu B, Pan Z, Ding D, Cuiuri D, Li H, Xu J, et al. A review of the wire arc additive manufacturing of metals: properties, defects and quality improvement. J Manuf Process 2018;35:127–39. doi:10.1016/j.jmapro.2018.08.001.

[19] Haibin Geng, Jinglong Li, Jiangtao Xiong, Xin Lin, Dan Huang FZ. Formation and improvement of surface waviness for additive manufacturing 5A06 aluminium alloy component with GTAW system. Rapid Prototyp J 2017;55. doi:10.1108/RPJ-04-2016-0064.

[20] Reeves PE. Reducing the surface deviation of Stereolithography components 1998.

[21] Luis Pérez CJ, Vivancos Calvet J, Sebastián Pérez MA. Geometric roughness analysis in solid free-form manufacturing processes. J Mater Process Technol 2001;119:52–7. doi:10.1016/S0924-0136(01)00897-4.

[22] Price S, Cheng B, Lydon J, Cooper K, Chou K. On Process Temperature in Powder-Bed Electron Beam Additive Manufacturing: Process Parameter Effects. J Manuf Sci Eng 2014;136:061019. doi:10.1115/1.4028485.

[23] Colegrove PA, Coules HE, Fairman J, Martina F, Kashoob T, Mamash H, et al. Microstructure and residual stress improvement in wire and arc additively manufactured parts through high-pressure rolling. J Mater Process Technol 2013;213:1782–91. doi:10.1016/j.jmatprotec.2013.04.012.

[24] Rangaswamy P, Griffith ML, Prime MB, Holden TM, Rogge RB, Edwards JM, et al. Residual stresses in LENS® components using neutron diffraction and contour method. Mater Sci Eng A 2005;399:72–83. doi:10.1016/j.msea.2005.02.019.

[25] Adjassoho B, Kozeschnik E, Lechner C, Habersohn C, Bleicher F, Gössinger S, et al. Controlled surface treatment with machine hammer peening. Met 2013 - 22nd Int Conf Metall Mater Conf Proc 2013;4:13–8.

[26] Hönnige JR, Colegrove P, Williams S. Improvement of microstructure and mechanical properties in Wire + Arc Additively Manufactured Ti-6Al-4V with Machine Hammer Peening. Procedia Eng 2018;216:8–17. doi:10.1016/j.proeng.2018.02.083.

[27] Tsuchida N, Tomota Y, Nagai K, Fukaura K. A simple relationship between L??ders elongation and work-hardening rate at lower yield stress. Scr Mater 2006;54:57–60. doi:10.1016/j.scriptamat.2005.09.011.

[28] Song R, Ponge D, Raabe D. Improvement of the work hardening rate of ultrafine grained steels through second phase particles. Scr Mater 2005;52:1075–80. doi:10.1016/j.scriptamat.2005.02.016.

[29] Hönnige JR, Colegrove PA, Ganguly S, Eimer E, Kabra S, Williams S. Control of residual stress and distortion in aluminium wire + arc additive manufacture with rolling. Addit Manuf 2018;22:775–83. doi:10.1016/j.addma.2018.06.015.

[30] Lee Y, Choi C. Driving Force for Austenite to Martensitic Transformation and Stacking Fault Energy of austenite in Fe-Mn Binary system 2000;31:355–60.

[31] Karaman I, Sehitoglu H, Chumlyakov YI, Maier HJ, Kireeva I V. Extrinsic stacking faults and twinning in Hadfield manganese steel single crystals. Scr Mater 2001;44:337–43. doi:10.1016/S1359-6462(00)00600-X.

[32] Hill DC, Passoja DE. Understanding the Role of Inclusions and Microstructure in Ductile Fracture. Weld J 1974:481–5.

[33] Sridharan N, Noakes MW, Nycz A, Love LJ, Dehoff RR, Babu SS. On the toughness scatter in low alloy C-Mn steel samples fabricated using wire arc additive manufacturing. Mater Sci Eng A 2018;713:18–27. doi:10.1016/j.msea.2017.11.101.

[34] Byun J, Shim J, Cho YW, Lee DN. Non-metallic inclusion and intragranular nucleation of ferrite in Ti-killed C – Mn steel. Acta Mater 2003;51:1593–606. doi:10.1016/S1359-6454(02)00560-8.

[35] Kirkhope KJ, Bell R, Caron L, Basu RI, Ma KT. Weld detail fatigue life improvement techniques. Part 2: Application to ship structures. Mar Struct 1999;12:477–96. doi:10.1016/S0951-8339(99)00031-3.

**List of Figures**



**List of Tables**

# Highlights

- High surface waviness is detrimental to the static and dynamic behaviour of as-deposited WAAM steel structure.
- The failure mechanism for the as-deposited condition is the macroscopic mechanism, whereas the microscopic mechanism is dominant for the machined condition.
- Compressive stress induced by rolling on the as-deposited condition reduces the surface waviness and produces a corresponding increase in mechanical strength and fatigue strength due to the macroscopic and microscopic influence.
- WAAM mild steel components could be used in the as-deposited condition for engineering application when rolling is applied to reduce its surface waviness.